


Mobility edges and fractal states in quasiperiodic Gross-Pitaevskii chains

Oleg I. Utesov^{1,*}, Yeongjun Kim^{1,2,†} and Sergej Flach^{1,2,‡}

¹Center for Theoretical Physics of Complex Systems, *Institute for Basic Science (IBS)*, Daejeon 34126, Korea

²Basic Science Program, *Korea University of Science and Technology (UST)*, Daejeon 34113, Korea

 (Received 6 June 2025; revised 2 October 2025; accepted 30 October 2025; published 21 November 2025)

We explore the properties of a Gross-Pitaevskii chain subject to an incommensurate periodic potential, i.e., a nonlinear Aubry-André model. We show that the condensate crucially impacts the properties of the elementary excitations. In contrast to the conventional linear Aubry-André model, the boundary between localized and extended states (mobility edge) exhibits nontrivial branching. For instance, in the high-density regime, “tongues” of extended phases at intermediate energies penetrate the domain of localized states. In the low-density case, the situation is opposite, and tongues of localized phases emerge. Moreover, intermediate critical (fractal) states are observed. The low-energy phonon part of the spectrum is robust against the incommensurate potential. Our study shows that accounting for interactions, already at the classical level, leads to highly nontrivial behavior of the elementary excitation spectrum.

DOI: [10.1103/d9sb-lj4k](https://doi.org/10.1103/d9sb-lj4k)

I. INTRODUCTION

While many years have passed since Anderson introduced the concept of localization [1], it continues to attract significant attention for good reasons [2–10]. The localization phenomenon is probed with new tools such as level spacing statistics (r ratios) [11,12], on new structures, including random regular [7,10] and irregular graphs [13,14], models with correlated disorder [15,16], etc. Furthermore, a whole new field of many-body localization emerged [17–21]. Nowadays, optical lattices of bosonic and fermionic atoms can be created, enabling the study and testing of important theoretical concepts, including localization. Experiments with disordered or quasiperiodic potentials have provided direct observation of Anderson localization [22,23], as well as the exploration of many-body localization through controlled interactions and disorder [24].

The Aubry-André (AA) model is one of the few models for which localization properties are known exactly [25–28]. This model consists of a simple nearest-neighbor hopping and an incommensurate on-site potential,

$$\mathcal{H}_{\text{AA}} = \sum_l (\varepsilon_l a_l^\dagger a_l - J a_{l+1}^\dagger a_l - J a_l^\dagger a_{l+1}), \quad (1)$$

$$\varepsilon_l = W \cos(2\pi\beta l + \varphi), \quad (2)$$

where the lattice parameter is set to unity, β is an irrational number (otherwise, Bloch’s theorem applies, and the system develops a band structure), and φ is an arbitrary phase, which becomes unimportant in the thermodynamic limit $N \rightarrow \infty$. Introducing the Fourier transform of the operators, one can

see that the problem in reciprocal space is dual to the original. The self-dual point $W_C = 2J$ separates the regimes of localized ($W > W_C$) and extended ($W < W_C$) states. At the critical point, all the states are fractal. Note that $4J$ is the bandwidth at $W = 0$. The model has been experimentally realized in ultracold atom systems and photonic lattices, which allow for observing localization transitions and fractal wave functions [23]. The AA model is also suitable for many-body generalizations [24,29–31], where quasiperiodicity can essentially modify the phase diagrams and stabilize exotic phases [32–36]. Notably, an incommensurate potential can result in a transition between Mott insulator and superfluid phases [37].

In the present study, we consider an extension of the standard AA model (1) by including an interaction on the classical level, thereby making the connection to the physics of Gross-Pitaevskii lattices (see, e.g., Refs. [38–42]). Moreover, the considered model can be viewed as a toy model for studying many-body localization physics in the presence of an incommensurate periodic perturbation. In previous crucial research [43,44], the mobility edge separating low-energy delocalized and high-energy localized states was predicted theoretically and observed experimentally. Notably, the mobility edge also emerges in relatively simple generalizations of the AA model [45–47]. Importantly, in Ref. [44], only the ground and one of the highly excited states were considered in a weakly interacting regime for two relatively small system sizes due to apparent experimental difficulties.

We perform a comprehensive study of the Bogoliubov-de Gennes (BdG) excitations of the model, emphasizing two qualitatively different regimes of low and high densities, equivalent to weak and strong interaction cases. In both cases, exploring the scaling properties with the system size N typically varied from $N \lesssim 10^3$ to $N \sim 10^4$, we observe peculiar behavior of the BdG excitations showing the nontrivial branching of mobility edges, separating the extended, fractal, and localized modes. In a certain domain of the W -excitation

*Contact author: utesov@gmail.com

†Contact author: yeongjun.kim.04@gmail.com

‡Contact author: sergejflach@googlemail.com

energy plane, one can observe “tongues” of the extended phase in the form of several narrow quasibands separated by wide localized regions and “reentrant” behavior upon W growth. We show that low-energy physics can be formulated in terms of acoustic modes subject to a renormalized AA potential governed by their wave number and W . This effective approach predicts that some low-energy modes remain delocalized regardless of the AA potential strength. This behavior contrasts with the standard AA model, where all eigenstates are localized when $W > W_C$. In the present case, one can introduce a quantity W_{NL} which indicates when some modes, usually the highest-energy excitations, start to localize upon W growth. In both low- and high-density regimes, we provide estimations for W_{NL} which are numerically shown to provide a semiquantitative level of accuracy.

II. GENERAL FORMULAS

We consider the following Hamiltonian,

$$\mathcal{H} = \sum_l \left[\varepsilon_l |\psi_l|^2 - J(\psi_{l+1}^* \psi_l + \psi_l^* \psi_{l+1}) + \frac{g}{2} |\psi_l|^4 \right], \quad (3)$$

where $l = 1 \dots N$, ψ_l is the condensate wave function on a site l (classical field), and ε_l is the Aubry-André on-site potential (2). In addition to the kinetic energy governed by J , there is the nonlinearity proportional to g . Model (3) with uncorrelated on-site disorder ε_l was considered in Ref. [9]; we adapt some ideas of that study for our purposes (see also Refs. [48,49] where generic disorder was considered and localization properties were studied). The equations of motion read $i\dot{\psi}_l = \partial \mathcal{H} / \partial \psi_l^*$ (see Appendix A for details).

Notably, the Hamiltonian preserves the number of particles $A = \sum_l |\psi_l|^2$. Therefore, we introduce a crucial system parameter, the density of particles $a = A/N$. We distinguish two regimes of low and high densities $ga \ll J$ and $ga \gg J$, respectively. It is pertinent to note that a variation of a is equivalent to a rescaling of the interaction g , so the two regimes correspond to weakly and strongly interacting cases. In all our numerical calculations, we use dimensionless parameters $J = g = 1$ [9], and vary a from small values to large ones covering both the above-mentioned regimes, as well as the intermediate case of $ga \sim J$. Unless stated otherwise, we set $\beta = (\sqrt{5} - 1)/2$ (inverse golden ratio) and use its rational approximations in numerics (see Appendix B).

A standard trick of introducing the chemical potential μ and $\mathcal{H}' = \mathcal{H} - \mu A$ [9] allows to formulate equations for the time-independent ground state G_l for a fixed number of particles A [43] (see Appendix A),

$$(\varepsilon_l - \mu)G_l - J(G_{l+1} + G_{l-1}) + g|G_l|^2 G_l = 0, \quad (4)$$

which implicitly define a as function of μ (and vice versa) and other parameters (e.g., for $W = 0$ one has $ga = \mu + 2J$). Next, we define the ground-state correlation field [9]

$$\zeta_l = \frac{G_{l+1} + G_{l-1}}{G_l}, \quad (5)$$

which is equal to 2 in the absence of the AA potential.

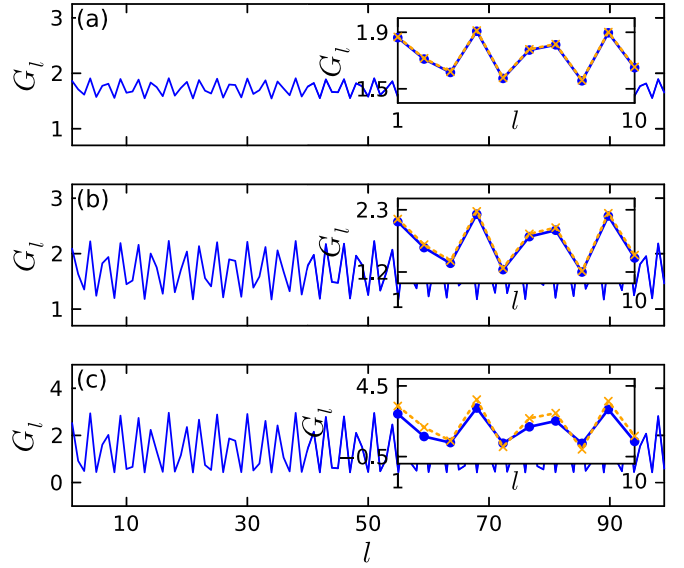


FIG. 1. The high-density regime ground-state amplitudes (we use blue lines instead of discrete dots for presentation purposes) for the chain size $N = 2584$. Here, $a = 3$ with (a) $W = 1$, (b) $W = 3$, and (c) $W = 10$. In the insets, we compare G_l 's and the linear response estimations (6) (dashed orange lines). Upon W growth, deviations from the linear response become apparent.

For small $W \ll \max(ga, J)$, the ground state varies following the quasiperiodic potential (linear response),

$$G_l \approx \sqrt{a} \left[1 - \frac{\varepsilon_l}{2ga + 2J(1 - \cos 2\pi\beta)} \right]. \quad (6)$$

However, for $W \gtrsim \max(ga, J)$, a strongly nonlinear response is expected.

We compute the ground state using the gradient descent method (see Appendix A) with a constraint $\sum_l |\psi_l|^2 = A$ (the Lagrange multiplier corresponds to the chemical potential μ). Figure 1 shows the numerically obtained G_l in the high-density regime ($a = 3$) for different potential values $W = 1, 3, 10$ in Figs. 1(a)–1(c), respectively. The insets display a close-up for $1 \leq l \leq 10$, compared with the linear response prediction (6). Evidently, the latter fails to accurately describe the ground state for strong AA potentials, namely for $W \gtrsim ga$ in the high-density regime. In the low-density regime, the same rule applies, but W should be compared with J (see Fig. 2). In particular, we use $a = 0.3$ and three various W . The linear response equation (6) works reasonably well for $W \sim 1$ in this case. For the highest $W = 10$, the ground-state response is essentially nonlinear, leading to weakly coupled condensate puddles. Nevertheless, the ground state is extended even for the strongest AA potential.

In Fig. 3, we examine the scaling of the ground-state participation number $P = (\sum_l G_l^2)^2 / \sum_l G_l^4$ for the same parameters a and W used in Fig. 2. The calculations are performed for system sizes N from 377 to 6765. The numerical results show $P \propto N$, indicating that the ground state is extended even for a strong quasiperiodic potential $W = 10$. This behavior may be understood as follows: for strong quasiperiodic perturbations and low densities, the condensate mostly occupies sites with the lowest on-site

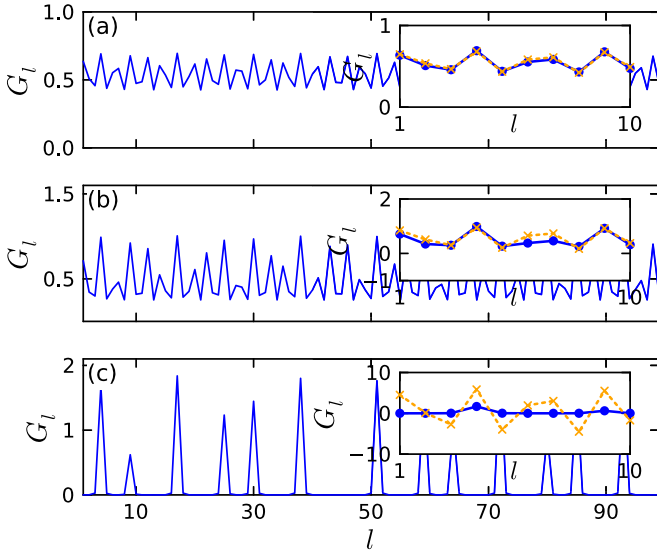


FIG. 2. The ground-state amplitudes for the density $a = 0.3$ and $N = 2584$ (low-density regime), for different AA potential strengths $W = 1, 3, 10$ from (a)–(c), respectively. All notations are identical to those of Fig. 1.

energy with $\cos(2\pi\beta l + \varphi) < -1 + \delta$ for some positive $\delta \ll 1$. Then, in the thermodynamic limit, the probability of the site to be occupied is $\sim \delta^{1/2}$ and these sites are quasihomogeneously spread along the chain.

Fluctuations above the ground state, i.e., BdG modes, are defined using the representation

$$\psi_l = G_l + \chi_l e^{-i\lambda t} - \Pi_l^* e^{i\lambda t}. \quad (7)$$

Here, λ is the energy of an excitation. This representation is valid for infinitesimal χ_l and Π_l in our classical approach since G_l is nonzero everywhere, even for strong AA potentials, and the ground state is extended. In the quantum case with $a \lesssim 1$ and $g \gtrsim J$, some sites are expected to have zero occupancy for strong enough AA, and the chain will be effectively decoupled. We do not consider such effects here. Moreover, a transition to the Mott insulator phase can occur, which is also beyond the scope of the present study.

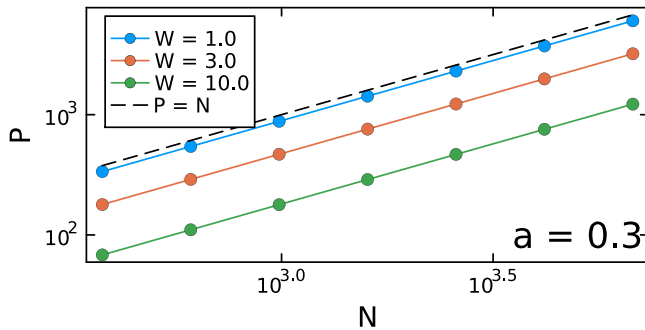


FIG. 3. Scaling of the participation number of the ground state P with N for $a = 0.3$ and $W = 1, 3, 10$. Even for the strongest AA potential, $W = 10$, the slope clearly indicates the delocalized nature of the ground state.

Linearizing the equations of motion in χ_l and Π_l fields, we get the BdG equations

$$\begin{aligned} \lambda \chi_l &= J \zeta_l \chi_l + g G_l^2 (\chi_l - \Pi_l) - J(\chi_{l+1} + \chi_{l-1}), \\ \lambda \Pi_l &= -J \zeta_l \Pi_l + g G_l^2 (\chi_l - \Pi_l) + J(\Pi_{l+1} + \Pi_{l-1}). \end{aligned} \quad (8)$$

Importantly, there is always a solution $\chi_l = \Pi_l \propto G_l$ for $\lambda = 0$ (the Nambu-Goldstone mode due to the global phase invariance breaking). There is also a particle-hole symmetry, so if λ_v corresponds to an eigenvector (χ_l^v, Π_l^v) then $-\lambda_v$ corresponds to the eigenvector (Π_l^v, χ_l^v) .

Further simplification can be made by introducing the sum and the difference of the fields $\chi_l = (S_l + D_l)/2$ and $\Pi_l = (S_l - D_l)/2$ (see Appendix A). Note that fields S_l and D_l have similar localization properties due to a local coupling between them. Excluding D_l , we have

$$\begin{aligned} E S_l &\equiv \frac{\lambda^2}{J} S_l = (J \zeta_l + 2g G_l^2)(\zeta_l S_l - S_{l+1} - S_{l-1}) \\ &\quad - J(\zeta_{l+1} S_{l+1} + \zeta_{l-1} S_{l-1} - S_{l+2} - 2S_l - S_{l-2}). \end{aligned} \quad (9)$$

This system of linear equations is suitable for numerical diagonalization for a given ground state G_l [and consequently, ζ_l from Eq. (5)]. Note that at $W = 0$ one has the Bogoliubov spectrum of excitations labeled by momentum $k \in (-\pi, \pi]$,

$$E_k = 4(1 - \cos k)[ga + (1 - \cos k)J], \quad (10)$$

and the “bandwidth” is $8(ga + 2J)$. The latter is mainly determined by J in the low-density regime and ga in the high-density one. As in the AA model, we show that W should be compared with the bandwidth to judge the localization on a qualitative level.

Localization properties of the eigenstates can be addressed using the participation number, which for the v th mode is defined as follows:

$$P_v = \frac{(\sum_l n_{l,v})^2}{\sum_l n_{l,v}^2}, \quad n_{l,v} = |\chi_{l,v}|^2 + |\Pi_{l,v}|^2. \quad (11)$$

The states are classified according to the scaling of their participation number with the system size. For extended states $P \sim N$, and for localized ones $P \sim N^0$. The fractal (critical) modes are characterized by $P \sim N^\tau$ with $0 < \tau < 1$. Numerically, τ is determined as the slope of the $\ln P(\ln N)$ function, which is approximately linear for extended and critical states.

Using the equations above, we can develop some intuition on the excitation properties. To do so, we utilize the linear response formula (6) for the ground state. In the low-density regime $ga \ll J$, for high-energy excitations we can neglect $g G_l^2 \Pi_l$ in Eqs. (8). It is easy to see that to zeroth order in ga/J one returns to the standard AA model, whereas the first correction renormalizes W . It reads

$$\Lambda = \left[1 - \frac{2ga}{J(1 - \cos 2\pi\beta)} \right] W. \quad (12)$$

For low-energy excitations, the terms $g G_l^2 (\chi_l - \Pi_l)$ in Eqs. (8) are crucial for linear dispersion at $W = 0$ and cannot be neglected. Therefore, we can expect that the condition $\Lambda = 2J$ indicates localization of the highest-energy modes

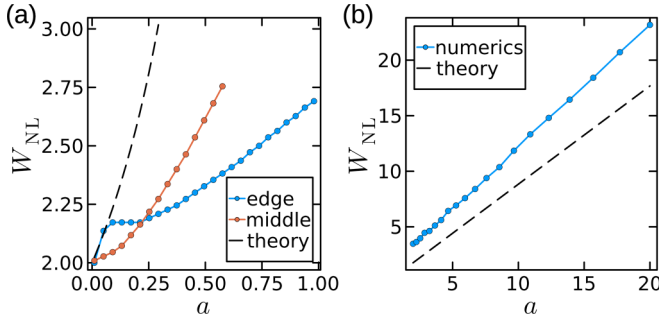


FIG. 4. In the nonlinear Aubry-André model (3), W_{NL} serves as an indicator when localized modes emerge upon W growth. It depends on the particle density a . Here, we plot it for (a) low-density and (b) high-density regimes. In (a), blue and red curves correspond to the emergence of the localized modes at the edge ($\lambda \approx 5$) and the middle ($\lambda \approx 2.5$) of the spectrum, respectively. In (b), only W_{NL} for the edge is presented. The dashed lines are theoretical predictions (13) and (19).

and determines W_{NL} . Using Eq. (12), one can write

$$W_{\text{NL}} \approx 2J \left[1 + \frac{2ga}{J(1 - \cos 2\pi\beta)} \right]. \quad (13)$$

One of the crucial observations is that this estimation works well only for the states near the edge of the spectrum for $a \ll 1$ [see Fig. 4(a)]. Counterintuitively, the states in the middle of the spectrum become localized first, which can be understood using the concept of localized phase tongues (see below).

In the high-density regime $ga \gg J$, we can rewrite Eqs. (9) in the approximate Aubry-André-like form with the effective constant being energy dependent. Using Eqs. (5) and (6), one obtains [9]

$$G_l \approx \sqrt{a} \left(1 - \frac{\varepsilon_l}{2ga} \right), \quad (14)$$

$$\zeta_l \approx 2 - \frac{1}{2ga} (\varepsilon_{l+1} + \varepsilon_{l-1} - 2\varepsilon_l). \quad (15)$$

The approximate equation for the BdG excitations (9) reads

$$ES_l = 2gG_l^2 (\zeta_l S_l - S_{l+1} - S_{l-1}). \quad (16)$$

Dividing (16) by $2gG_l^2$, and collecting terms up to the first order in ε_l/ga , we get

$$E'S_l = -(S_{l+1} + S_{l-1}) - \Lambda(E) \cos(2\pi\beta l + \varphi) S_l, \quad (17)$$

which corresponds to the standard AA model (1) with renormalized E -dependent potential $\Lambda(E)$. Here,

$$E' = \frac{E - 4ga}{2ga}, \quad \Lambda(E) = \left[\frac{E}{2ga} - 1 + \cos(2\pi\beta) \right] \frac{W}{ga}. \quad (18)$$

Near the edge of the spectrum $E_{\text{max}} \approx 8ga$ (10), the AA critical point condition $\Lambda(E_{\text{max}}) = 2$ yields

$$W_{\text{NL}} \approx \frac{2ga}{3 + \cos 2\pi\beta}. \quad (19)$$

Therefore, localization of high-energy modes requires $W \sim ga$, which, formally, places the system in the regime where the linear response theory for the ground state (6) is inapplicable. However, in Fig. 4(b), we show that the estimate (19) agrees with the numerical result on a semiquantitative level of accuracy. This is likely because the linear response is surprisingly accurate beyond the $W \ll ga$ parameter domain as shown in Fig. 2(b). Note also that Eq. (18) hints at the existence of the mobility edge in the spectrum for $W > W_{\text{NL}}$. Another important feature is the mobility edge β dependence, which is briefly discussed in Appendix C.

III. SPECTRUM AND MOBILITY EDGES

The complex nature of the BdG spectrum of model (3) in the case of uncorrelated disorder was shown in Ref. [9]. The divergence of the localization length was observed not only for low-energy excitations, but also for modes near a certain energy, which depends on the particle density. The nonlinear Aubry-André model also exhibits nontrivial spectral properties, as shown in Fig. 5. In Figs. 5(a)–5(d), we show the evolution of the BdG excitation spectra with W for various particle densities. The color encodes the fractal dimensions of the respective states. Roughly, one can see that in agreement with the discussion above, the high-density spectra develop the mobility edge at certain values of W , which moves to lower energies upon further growth of W . Moreover, the lowest-energy modes are delocalized even for the largest W values.

However, a deeper view reveals the fine structure of the spectra for certain intermediate W ranges (depending on a). For instance, in Fig. 5(e), we consider the section of Fig. 5(d) for $a = 15$ along the vertical line $W = 23$. While the low- and high-energy modes are delocalized and localized, respectively, for intermediate λ we have a mixing of “subbands” of localized and delocalized states and, thus, multiple mobility edges. Notably, multiple mobility edges were also observed theoretically for disordered Bose superfluids in Ref. [6] and for generalized Aubry-André-like models in Refs. [50,51]. The connection between the latter studies and the present model is discussed in Appendix D.

For large enough W , a single mobility edge separates low-energy (modulated) plane waves and high-energy localized modes [see Figs. 5(f)–5(j)]. Moreover, intermediate critical fractal states can be observed (see Appendix E for the relation to the extended Harper model famous for the emergence of the fractal states). The difference among the three types of modes is apparent in Figs. 5(h)–5(j).

For the high-density regime, multiple mobility edges originate from extended phase tongues, which persist in the form of narrow subbands separating localized phase regions. This idea is illustrated in detail in Fig. 6.

Physics is also far from being trivial in the low-density regime. Here, the mobility-edge tongues (wedged regions) protrude toward lower W , unlike in the high-density regime, where the tongues protrude toward higher W . They evolve differently at the spectrum’s middle part and edges as W increases, as shown in the red (edge) and blue (middle) curves of Fig. 4(a). The full-spectrum map appears in Fig. 5(a). In particular, states remain extended near the center, localized at intermediate energies, and extended again at the upper edge.

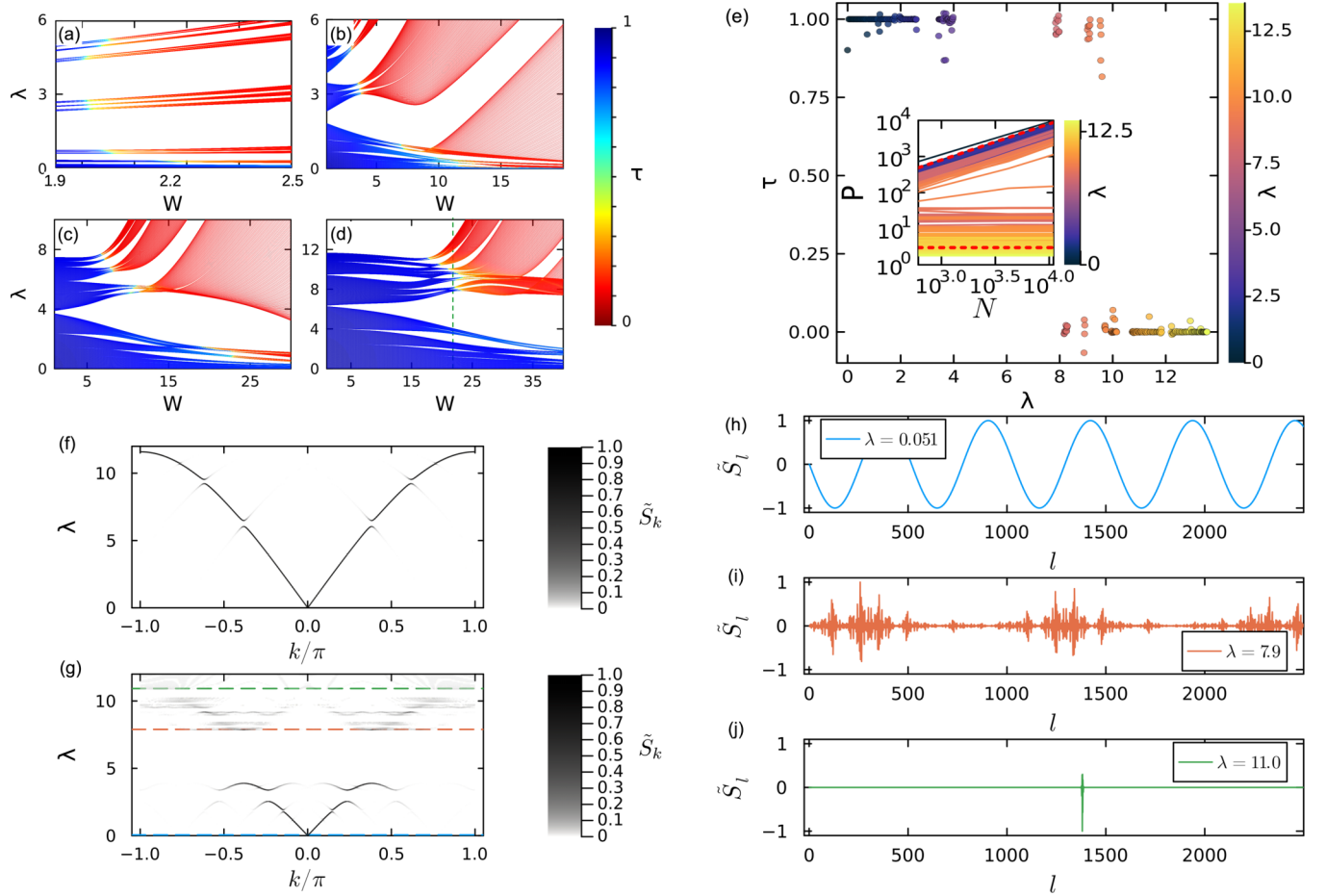


FIG. 5. Overview of the nonlinear Aubry-André model (3) properties. In (a)–(d), we show elementary excitations spectra for the particle densities $a = 0.01, 1, 5, 15$ and the system size $N = 2584$, respectively, and τ , which indicates the corresponding participation number scaling properties. In (e), we present $\tau(\lambda)$ for $W = 23$ [vertical section of (d)], which reveals multiple mobility edges. For the scaling analysis we used $N = 987, 1597, 2584$, and τ was averaged over a small energy window $\delta\lambda = 0.01$. The inset shows the scaling of P vs N on a log-log plot. Dashed red lines indicate reference scalings $P = N^1$ and $P = N^0$. Further insights into the model properties can be obtained using reciprocal space wave functions. In (f) and (g), we contrast spectra for $a = 3$ with respective $W = 3$ and $W = 10$. In the former case, all the modes are delocalized, having well-resolved k -space peaks, whereas in the latter case, the localization emerges through an intermediate fractal regime. The corresponding wave functions—extended, critical, and localized—for $\lambda = 0.051, 7.9$, and 11 are shown in (i)–(k), respectively ($N = 2584$).

IV. EFFECTIVE LOW-ENERGY THEORY

Since the pioneering work by Bogoliubov [52], it is well known that in a dilute Bose gas, low-energy excitations essentially differ from the high-energy ones. The former are hydrodynamic phonons (acoustic waves), whereas the latter are nearly free bosons. We observe that in our theory, this property is crucial.

In our model, the Nambu-Goldstone mode is characterized by $S_l \propto G_l$ and $D_l = 0$. It is natural to expect that smooth low-energy solutions can be obtained by introducing variables $\tilde{S}_l = S_l/G_l$ and $\tilde{D}_l = D_l/G_l$. Indeed, the corresponding excitation real-space profiles of \tilde{S}_l exhibit plane-wave-like behavior even for large W for which the rest of the spectrum is localized [see Figs. 5(g) and 5(h)].

To understand the physics behind such a behavior, we rewrite Eq. (9) using $\lambda = i\partial_t$ and a gradient expansion of smooth \tilde{S}_l . In more detail, we use

$$\tilde{S}_{l\pm 1} = (\tilde{S} \pm \partial_x \tilde{S} + \frac{1}{2} \partial_x^2 \tilde{S})|_{x=l}. \quad (20)$$

After some calculations, Eq. (9) can be transformed to

$$\partial_t^2 \tilde{S} = f_l \partial_x^2 \tilde{S} + g_l \partial_x \tilde{S}. \quad (21)$$

Here,

$$f_l = JgG_l^2 \zeta_l + J^2 \left(1 + \frac{\zeta_l^2}{2} - \frac{3\zeta_l^{(2)}}{2} \right), \quad (22)$$

$$g_l = 2JgG_l^2 \xi_l + J^2 (\zeta_l \xi_l^{(1)} - \xi_l^{(2)}) \zeta_l, \quad (23)$$

with

$$\zeta_l^{(n)} = \frac{G_{l+n} + G_{l-n}}{G_l}, \quad \xi_l^{(n)} = \frac{G_{l+n} - G_{l-n}}{G_l}. \quad (24)$$

Importantly, for $W = 0$, $f_l = 2Jga$ and $g_l = 0$, so excitations are acoustic waves with $\lambda^2 = 2Jgak^2$, which is just a long-wavelength expansion of Eq. (10). More insights can be obtained from the perturbative expansion (6). For example, in

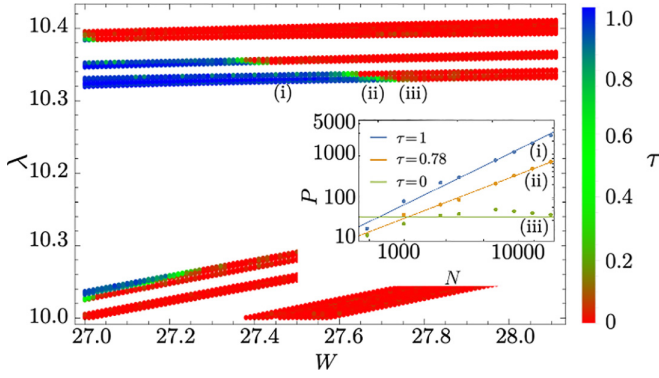


FIG. 6. For a given density a (here, $a = 18$) the phase diagram on the W - λ plane has nontrivial branching due to the tongues. In the high-density regime, the tongues of the delocalized phase penetrate the localized phase domain in the form of several narrow quasibands. At the tongue ends, fractal states (green dots) can be observed. The inset shows the scaling of the participation ratio for the states indicated by labels (i)–(iii). Exponent τ reveals their respective extended, fractal, and localized nature. System sizes are from $N = 377$ to $N = 46\,368$.

the high-density regime, one has

$$f_l \approx 2Jga - (1 + \cos 2\pi\beta)JW \cos(2\pi\beta l + \varphi), \quad (25)$$

$$g_l \approx 2 \sin 2\pi\beta JW \sin(2\pi\beta l + \varphi). \quad (26)$$

We see that f_l and g_l are similar to the initial AA potential, which mixes harmonics with k differing by $2\pi\beta$. In general, perturbation to f_l , δf_l , and g_l contain higher-order harmonics, for example, $\pm 4\pi\beta$ with coefficient $\propto W^2$ and others [43]. In more detail, for $W \neq 0$, δf_l and g_l can be represented as sums of terms $\propto W^n \cos n(2\pi\beta l + \varphi)$ and $\sin n(2\pi\beta l + \varphi)$, respectively ($n \geq 1$). However, they are coupled to derivatives of \tilde{S} in the equation of motion. So, after the Fourier transform, we have a problem similar to the original Aubry-André one,

$$(\omega^2 - c^2 k^2) \tilde{S}(\omega, k) + \sum_{n \neq 0} [k_n^2 f_n + ik_n g_n] \tilde{S}(\omega, k_n) = 0, \quad (27)$$

where $k_n = k - 2\pi n\beta$. The last terms here “mix” states with various momenta which differ by $2\pi\beta$. It is easy to see (using, e.g., the second-order perturbation theory) that the correction means that the effective AA parameter $\Lambda \propto kW$ and regardless of how strong is the original W , for small enough energies, the BdG modes will be extended.

Numerically, we observe that low-energy excitations are only weakly perturbed [see Figs. 5(f) and 5(g)]. However, with the energy growth, the admixture of higher harmonics becomes tangible. Even for strong enough W the whole first “quasiband” (with $k \in (-\pi\beta, \pi\beta]$ for $\beta < 1/2$ or $k \in (-\pi(1-\beta), \pi(1-\beta)]$ for $\beta > 1/2$) can be in the delocalized phase. This statement is illustrated in Fig. 5(g) for $a = 3$ and $W = 10$, where states below the largest gap have only several significant Fourier harmonics, and we can ascribe them the momentum in $k \in (-0.38\pi, 0.38\pi)$ interval (here, $1 - \beta \approx 0.38$).

V. CONCLUSION

We studied the localization properties of the Bogoliubov-de Gennes modes of the nonlinear Aubry-André model based on the bosonic Gross-Pitaevskii lattice in both low- and high-density regimes. In our classical approach, they are equivalent to weakly and strongly interacting cases. Unlike the usual Aubry-André model, where there is one critical value $W_C = 2J$ of the potential strength, which separates regimes of localized and extended states, the spectrum of normal modes possesses a mobility edge [43,44]. We report on its highly nontrivial behavior. In the high-density regime, in accordance with general arguments, localization first occurs at the edge of the spectrum for high-energy excitations. However, upon further increase of W , we reveal a peculiar branching of the mobility edge due to the tongues of delocalized phases penetrating the localized phase region. In the low-density regime, counterintuitively, the localization transition first occurs in the middle of the spectrum. This phenomenon is intimately related to the existence of the tongues of the localized phase penetrating the delocalized phase for $W \gtrsim 2$. At the tongues’ ends, as a rule, critical (fractal) states can be observed. Finally, the low-energy part of the spectrum is “protected” from localization. This issue can be addressed using the effective low-energy theory, which shows that the corresponding modes feel the renormalized Aubry-André potential.

ACKNOWLEDGMENTS

We are grateful to Boris Altshuler, Alexei Andreanov, and Tilen Cadez for valuable discussions. Financial support from the Institute for Basic Science (IBS) in the Republic of Korea through Project No. IBS-R024-D1 is acknowledged.

DATA AVAILABILITY

The data that support the findings of this article are not publicly available. The data are available from the authors upon reasonable request.

APPENDIX A: OBTAINING THE GROUND STATE AND BOGOLIUBOV-DE GENNES EQUATIONS

For the Hamiltonian (3), the equations of motion read

$$i\dot{\psi}_l = \frac{\partial \mathcal{H}}{\partial \psi_l^*} = \varepsilon_l \psi_l - J(\psi_{l+1} + \psi_{l-1}) + g|\psi_l|^2 \psi_l. \quad (A1)$$

We need to obtain the normalized ground state G_l with A particles. To do so, we write the normalized wave function

$$\tilde{\psi}_l = \frac{1}{\sqrt{A}} \psi_l. \quad (A2)$$

The Hamiltonian in terms of the normalized wave function is

$$\tilde{\mathcal{H}} \equiv \mathcal{H}/A = \sum_{l=1}^N \left[\varepsilon_l |\tilde{\psi}_l|^2 - J(\tilde{\psi}_l \tilde{\psi}_{l+1}^* + \tilde{\psi}_l^* \tilde{\psi}_{l+1}) + \frac{\tilde{g}}{2} |\tilde{\psi}_l|^4 \right], \quad (A3)$$

where we define $\tilde{g} = gA$.

The ground state has a minimal energy with constraint $\sum_l |\tilde{\psi}_l|^2 = 1$. Corresponding G_l ’s are obtained when the

following gradient becomes zero:

$$\nabla \mathcal{L} \equiv \nabla \left[\mathcal{H} - \mu \left(\sum_l |\tilde{\psi}_l|^2 - 1 \right) \right] = 0. \quad (\text{A4})$$

Here, we introduce the Lagrange multiplier μ (chemical potential). This gives the equations

$$(\varepsilon_l - \mu)\tilde{\psi}_l + g|\tilde{\psi}_l|^2\tilde{\psi}_l - J(\tilde{\psi}_{l+1} + \tilde{\psi}_{l-1}) = 0. \quad (\text{A5})$$

The ground-state problem can be solved using the gradient descent method, which we implement in the following form:

$$(\nabla \mathcal{L})_t = \frac{\nabla \mathcal{L} - (\nabla \mathcal{L} \cdot \tilde{\psi})\tilde{\psi}}{\|\nabla \mathcal{L} - (\nabla \mathcal{L} \cdot \tilde{\psi})\tilde{\psi}\|}. \quad (\text{A6})$$

Here, $(*)_t$ and $(*)_n$ are parallel, and normal components of the gradient to the unit sphere of norm 1. The gradient descent must be restricted to this unit sphere. The update is done (while conserving its norm) as

$$\tilde{\psi}^{(k+1)} = \cos(\phi_k)\tilde{\psi}^{(k)} - \sin(\phi_k)\nabla \mathcal{L}, \quad (\text{A7})$$

with a parameter step length ϕ_k as in the conventional gradient descent method. Note that the updated Eq. (A7) preserves the norm, but due to numerical instability, one still needs to perform normalization every few steps. At the ground state, the tangent component $(\nabla \mathcal{H})_t$ becomes zero; on the other hand, the normal component satisfies

$$(\nabla \mathcal{H})_n = \mu \nabla \|\tilde{\psi}\|^2 = 2\mu\tilde{\psi}. \quad (\text{A8})$$

Note that the obtained ground state has $G_l > 0$ on each site.

The Bogoliubov–de Gennes modes are weak excitations on top of the ground state,

$$\psi_l = G_l + \chi_l e^{-i\lambda l} - \Pi_l^* e^{i\lambda l}, \quad (\text{A9})$$

where $|\chi_l|, |\Pi_l| \ll G_l$. Using Eqs. (A1) and the chemical potential, one obtains Eqs. (8). They can be conveniently rewritten for $S_l = \chi_l + \Pi_l$ and $D_l = \chi_l - \Pi_l$ as

$$\lambda S_l = (J\zeta_l + 2gG_l^2)D_l - J(D_{l+1} + D_{l-1}), \quad (\text{A10})$$

$$\lambda D_l = J\zeta_l S_l - J(S_{l+1} + S_{l-1}). \quad (\text{A11})$$

D_l 's can be easily excluded, and we arrive at Eqs. (9) for S_l 's only.

APPENDIX B: FINITE-SIZE SCALING, RATIONAL APPROXIMATIONS, AND PHASE

In our calculations throughout the manuscript, we use chains of finite size with periodic boundary conditions for the Aubry-André potential

$$\varepsilon_l = W \cos(2\pi\beta l + \varphi). \quad (\text{B1})$$

Since we are mostly interested in $\beta = (\sqrt{5} - 1)/2$, it is natural to use its rational approximation in the form of ratios of Fibonacci numbers

$$\beta \approx \frac{F_{n-1}}{F_n}, \quad (\text{B2})$$

which suggests using, e.g.,

$$\beta = \frac{610}{987}, \frac{1597}{2584}, \frac{6765}{10946}, \dots \quad (\text{B3})$$

The denominators here represent natural choices for the system sizes: $N = 987, 2584, \dots$. This set of system sizes allows us to check scaling properties of eigenstates and to determine corresponding fractal dimensions (see Fig. 7).

Another important issue for the Aubry-André problem is the possible dependence of physics on the phase variable φ (see, e.g., Ref. [53]). In Fig. 7, we show this is not the case for our model. Even though near the transition point the standard deviation of participation ratio exponent τ slightly increases, we clearly observe the change of behavior from extended to localized for high-energy modes at W_{NL} .

APPENDIX C: OTHER VALUES OF PARAMETER β

We briefly discuss the results for other values of β . Qualitatively, the above discussion also applies here. Importantly, unlike the AA chain, the mobility edge is expected to depend on β , as inferred from the low-density (13) and high-density (19) approximations. This allows us to draw colorful Hofstadter butterflies [54] in Fig. 8. It shows the participation number scaling of the BdG spectrum λ vs β , with the predicted mobility edge (19) shown by a black line. We find that the mobility edges are indeed β dependent. However, as expected, the deviation from the analytical estimation arises because the high-density approximation assumes $ga \gg W$.

APPENDIX D: RELATION TO OTHER EXTENSIONS OF THE AUBRY-ANDRÉ MODEL

Some generalizations of the standard AA were considered in detail in Refs. [46,51]. Among them, there are models including next-nearest-neighbor hopping accompanied by higher harmonics for the incommensurate potential, e.g.,

$$W_2 \cos 2(2\pi\beta l + \phi), \quad (\text{D1})$$

as well as more complicated forms

$$\varepsilon_l = 2W \frac{\cos(2\pi\beta l + \varphi)}{1 - \alpha \cos(2\pi\beta l + \varphi)}. \quad (\text{D2})$$

Notably, for the latter case, the mobility edge is given by a simple analytical equation (see Ref. [46] for details),

$$\alpha\lambda = 2 \operatorname{sgn}(W)(1 - |W|/2). \quad (\text{D3})$$

Below, we show that the elementary excitations spectrum of the Gross-Pitaevskii chain can be approximately reproduced in similar “hybrid” models. However, in the interesting parameter ranges, they are essentially complex. We begin with the low-density regime, in the case when the localized phase tongue separates low- and high-energy delocalized excitations. The generic physics can be illustrated using $a = 0.05$ and $W = 2.05$. The $\lambda > 0$ part of the BdG spectrum can be accurately described using the equation [see Eqs. (8) and discussion below]

$$\lambda\chi_l = (J\zeta_l + gG_l^2)\chi_l - J(\chi_{l+1} + \chi_{l-1}). \quad (\text{D4})$$

The nontrivial part is evidently hidden in the $J\zeta_l + gG_l^2$ coefficient. Notably, for the parameters above, we can represent it

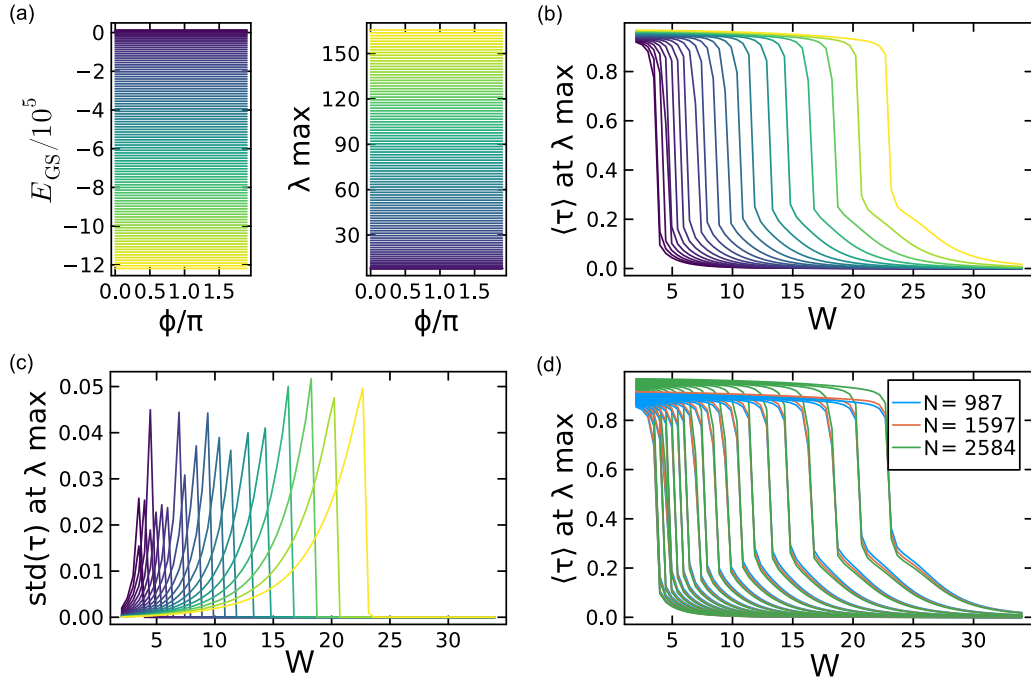


FIG. 7. Here, the range of $a \in (2, 20)$ is scanned (high-density regime), which corresponds to colors from violet to yellow in (a)–(c). (a) There is almost no ϕ -induced variation for the ground-state energy and maximal eigenvalue. (b) Averaged over ϕ participation ratio exponent τ clearly indicates localization transition at the edge of the spectrum. (c) Standard deviation of τ essentially increases at near the transition point. (d) Scaling of the participation ratio exponent with the system size; for curve bunches from left to right, a changes from 2 to 20.

as a Fourier series

$$J\zeta_l + gG_l^2 = \Lambda_0 + \Lambda_1 \cos(2\pi\beta l + \varphi) + \Lambda_2 \cos 2(2\pi\beta l + \varphi) + \Lambda_3 \cos 3(2\pi\beta l + \varphi) + \dots, \quad (\text{D5})$$

where we obtained numerically

$$\begin{aligned} \Lambda_0 &\approx 2.61, & \Lambda_1 &\approx 1.93, \\ \Lambda_2 &\approx 0.08, & \Lambda_3 &\approx -0.06. \end{aligned} \quad (\text{D6})$$

According to the coefficient values, the first idea should be to take only the first two terms. However, it is equivalent to the

standard AA model, and since $\Lambda_1 < 2$, it cannot capture localization at all. This highlights the crucial role of weaker higher harmonics. Notably, despite expansion (D5) being slowly convergent, inclusion of terms $\propto \Lambda_{2,3}$ is sufficient to semi-quantitatively reproduce the spectrum properties (see Fig. 9). One can also try to leave only one of the $\Lambda_{2,3}$ harmonics. We observed that this leads to an inaccurate description of the model spectrum. Noteworthy, our result here resembles the one shown in Fig. 3(a) of Ref. [51] for the AA model enhanced with weak next-nearest-neighbor hopping and weak second- and third-order incommensurate perturbations.

We proceed with the high-density regime. Below, we show that the most interesting case with multiple mobility edges can

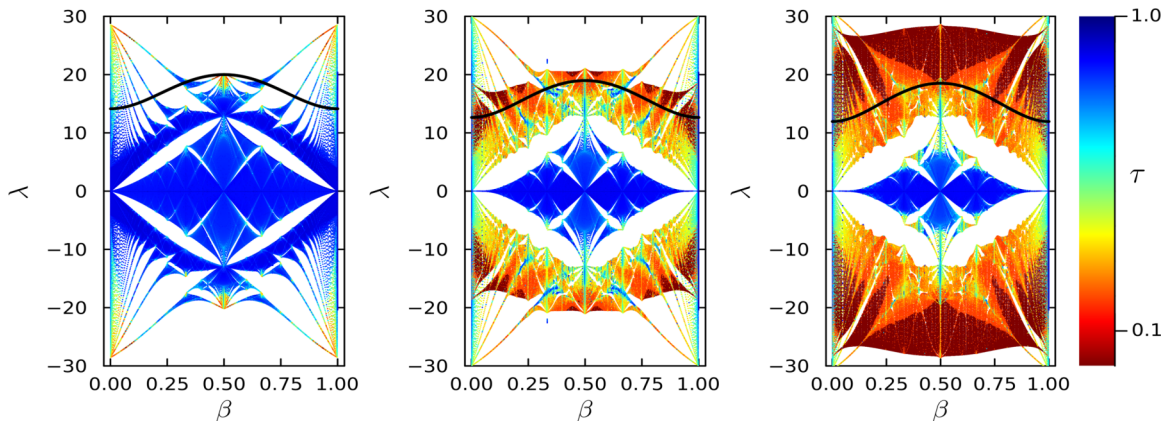


FIG. 8. The mobility edge β dependence. Here, $N = 987$, $a = 50$, $W = 50, 62.5, 75$ from left to right. The black line shows the analytical prediction for the mobility edge at the high-density regime (18).

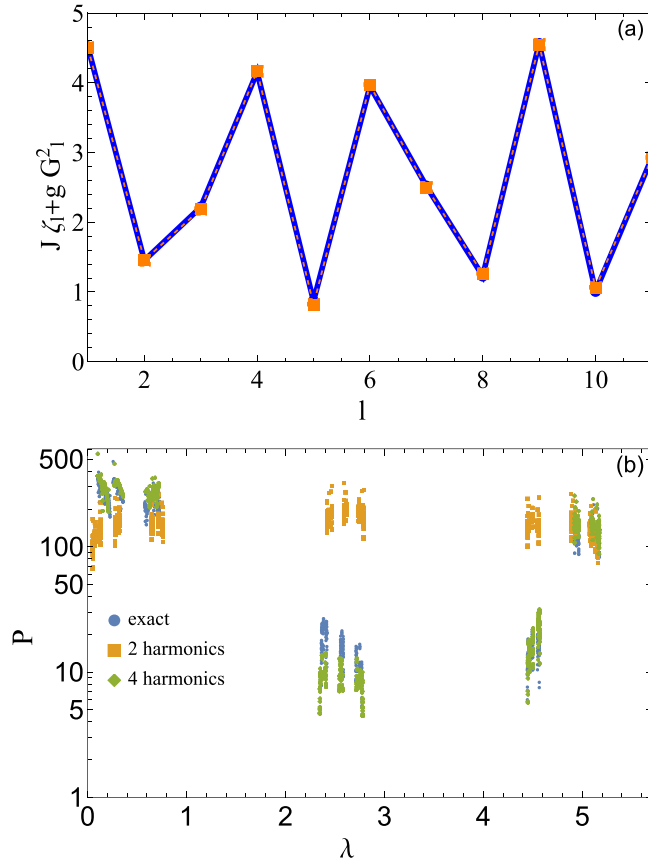


FIG. 9. In the low-density regime, the spectrum can be obtained using Eqs. (D4). (a) Description of $J\zeta_l + gG_l^2$ (blue dots) using Fourier harmonics (orange dots) can be sufficiently accurate. Here, four harmonics were used [see Eq. (D5)]. (b) The spectrum consists of localized modes in the middle (participation ratio $P \lesssim 50$ and delocalized modes at low and high energies as shown by blue dots representing the result of numerical diagonalization of the system of equations (D4). Simplified description using only two dominant harmonics is not sufficient (orange dots), whereas four harmonics reproduce the spectrum properties semiquantitatively (green dots). Here, $N = 987$, $a = 0.05$, $W = 2.05$.

be quantitatively discussed in terms of a particular multiharmonic model. For illustration purposes, we take $a = 18$ and $W = 27.5$ (cf. Fig. 6) and use Eq. (9). It can be diagonalized as is, but we want to make connections with AA-like models. To do so, we neglect small next-nearest-neighbor hoppings J , substitute $\zeta_{l\pm 1}$ with ζ_l , and arrive at

$$\frac{E}{2(gG_l^2 + J\zeta_l)} S_l = \frac{\zeta_l(2gG_l^2 + J\zeta_l)}{2(gG_l^2 + J\zeta_l)} S_l - S_{l+1} - S_{l-1}. \quad (\text{D7})$$

The exact spectrum (remember that $\lambda = \sqrt{EJ}$) is compared with the spectrum obtained using this equation in Fig. 10(a). Reasonable agreement can be reported. Next, we try to represent coefficients of Eq. (D7) in the form suggested in Refs. [46,51]. We write approximate expressions

$$\begin{aligned} \frac{1}{2(gG_l^2 + J\zeta_l)} &\approx a_0 + a_1 \cos(2\pi\beta l + \varphi) \\ &+ a_2 \cos 2(2\pi\beta l + \varphi) \\ &+ a_3 \cos 3(2\pi\beta l + \varphi) + \dots, \end{aligned}$$

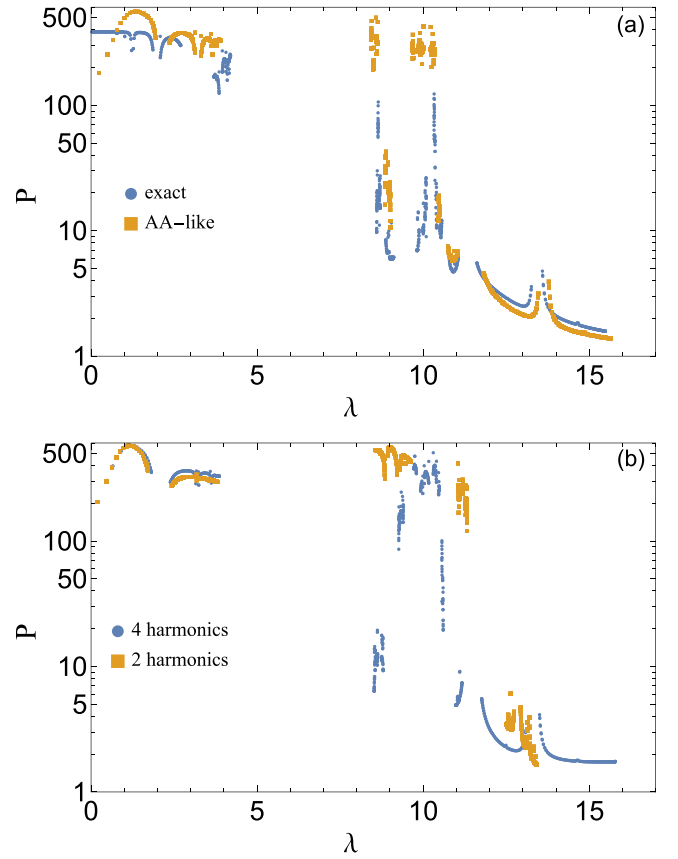


FIG. 10. In the high-density regime, the spectrum can be calculated using Eqs. (9). (a) Here, we compare the exact spectrum and the one obtained using the AA-like equation (D7). Despite certain discrepancies, the latter allows for describing multiple mobility edges. (b) Here, we compare two-harmonic and four-harmonic approximations [see Eq. (D8)]. The latter shows two mobility edges; however, the spectrum is somewhat different from those shown in panel (a). The model parameters are $N = 987$, $a = 18$, $W = 27.5$.

$$\begin{aligned} a_0 &\approx 0.029, & a_1 &\approx 0.018, \\ a_2 &\approx -0.004, & a_3 &\approx 0.009, \end{aligned} \quad (\text{D8})$$

$$\begin{aligned} \frac{\zeta_l(2gG_l^2 + J\zeta_l)}{2(gG_l^2 + J\zeta_l)} &\approx b_0 + \frac{b_1 \cos(2\pi\beta l + \varphi)}{1 - b_2 \cos(2\pi\beta l + \varphi)}, \\ b_0 &\approx 1.78, & b_1 &\approx 2.16, & b_2 &\approx 0.62. \end{aligned} \quad (\text{D9})$$

The latter representation works much better than a simple Fourier expansion. We compare the results for two and four harmonics in Eq. (D8) in Fig. 10(b). A Two-harmonic approximation yields only a single mobility edge, whereas the four-harmonic one yields two. Nevertheless, even in the latter approach, the spectrum structure is essentially different from that of the exact equation diagonalization. Finally, we note certain similarities between the obtained spectrum and the one shown in Fig. 3(b) of Ref. [51] obtained in a much simpler model.

To conclude, we showed that in the most interesting regimes, functions G_l and ζ_l are strongly modulated and nonperturbative, and the corresponding effective models

describing the spectrum cannot be represented in solvable forms with sufficient accuracy. Thus, the considered quasiperiodic Gross-Pitaevskii chain is characterized by more complex behavior in comparison with previously addressed generalizations of the AA model [46,50,51].

APPENDIX E: RELATION TO THE EXTENDED HARPER MODEL

This model was studied, e.g., in Refs. [55–57]. Here, we will mostly follow the notations of Ref. [57]. We show that for the high-density regime, the equations describing BdG excitations [Eq. (9)] correspond to the extended Harper model (EHM) ones. Importantly, this property hints at the possibility of observing fractal states in our model.

At high density, we can write

$$ES_l = 2gG_l^2(\zeta_l S_l - S_{l+1} - S_{l-1}). \quad (\text{E1})$$

Let us define the following operators,

$$\begin{aligned} \hat{D} &= \sum_l 2gG_l^2 |l\rangle\langle l|, \\ \hat{H}_0 &= \sum_l \zeta_l |l\rangle\langle l| - |l\rangle\langle l+1| - |l+1\rangle\langle l|. \end{aligned} \quad (\text{E2})$$

Then, we can write Eq. (E1) as follows,

$$E|S\rangle = (\hat{D}\hat{H}_0)|S\rangle, \quad (\text{E3})$$

where $|S\rangle = \sum_l S_l |l\rangle$. Performing the similarity transformation with $\hat{D}^{1/2}$ leads to effective BdG Hamiltonian

$\hat{D}^{1/2}\hat{H}_0\hat{D}^{1/2}$, which is Hermitian. So, after this transformation, the BdG equations are given by

$$E\tilde{S}_l = (h_l + h_{l-1})\tilde{S}_l - h_l\tilde{S}_{l+1} - h_{l-1}\tilde{S}_{l-1}, \quad (\text{E4})$$

where $\tilde{S}_l = (2g)^{-1/2}S_l/G_l$, and $h_l = 2gG_lG_{l+1}$, which approximately reads

$$h_l = 2ga - W \cos(\pi\beta)(e^{2\pi i(\beta l + \beta/2)} + e^{-2\pi i(\beta l + \beta/2)}). \quad (\text{E5})$$

With an appropriate rescaling, we have the extended Harper model with parameters given by

$$\begin{aligned} \lambda_2 &= \frac{ga}{W \cos^2(\pi\beta)}, \\ \lambda_1 &= \lambda_3 = \frac{1}{2|\cos(\pi\beta)|}. \end{aligned} \quad (\text{E6})$$

The phase diagram of the extended Harper model is known exactly [57].

In our model, we obtain

$$\begin{aligned} ga &> W|\cos(\pi\beta)| \quad \text{extended}, \\ ga &< W|\cos(\pi\beta)| \quad \text{critical}. \end{aligned} \quad (\text{E7})$$

These inequalities suggest the existence of fractal states in the spectrum of the nonlinear Aubry-André model; however, in the range of W where the whole procedure leading to Eq. (E4) is questionable (it relies on the $W \ll ga$ condition). Moreover, from the inequalities above, we cannot obtain any information related to mobility edges and localized states.

-
- [1] P. W. Anderson, Absence of diffusion in certain random lattices, *Phys. Rev.* **109**, 1492 (1958).
 - [2] *50 Years Of Anderson Localization*, edited by E. Abrahams (World Scientific Press, Singapore, 2010).
 - [3] F. Evers and A. D. Mirlin, Anderson transitions, *Rev. Mod. Phys.* **80**, 1355 (2008).
 - [4] Y. M. Beltukov, V. I. Kozub, and D. A. Parshin, Ioffe-Regel criterion and diffusion of vibrations in random lattices, *Phys. Rev. B* **87**, 134203 (2013).
 - [5] K. Slevin and T. Ohtsuki, Critical exponent for the Anderson transition in the three-dimensional orthogonal universality class, *New J. Phys.* **16**, 015012 (2014).
 - [6] S. Lellouch, L.-K. Lim, and L. Sanchez-Palencia, Propagation of collective pair excitations in disordered Bose superfluids, *Phys. Rev. A* **92**, 043611 (2015).
 - [7] K. S. Tikhonov and A. D. Mirlin, From Anderson localization on random regular graphs to many-body localization, *Ann. Phys.* **435**, 168525 (2021).
 - [8] D. A. Conyuh and Y. M. Beltukov, Random matrix approach to the boson peak and Ioffe-Regel criterion in amorphous solids, *Phys. Rev. B* **103**, 104204 (2021).
 - [9] Y. Kati, M. V. Fistul, A. Y. Cherny, and S. Flach, Anderson localization of excitations in disordered Gross-Pitaevskii lattices, *Phys. Rev. A* **104**, 053307 (2021).
 - [10] C. Vanoni, B. L. Altshuler, V. E. Kravtsov, and A. Scardicchio, Renormalization group analysis of the Anderson model on random regular graphs, *Proc. Natl. Acad. Sci. USA* **121**, e2401955121 (2024).
 - [11] V. Oganessian and D. A. Huse, Localization of interacting fermions at high temperature, *Phys. Rev. B* **75**, 155111 (2007).
 - [12] Y. Y. Atas, E. Bogomolny, O. Giraud, and G. Roux, Distribution of the ratio of consecutive level spacings in random matrix ensembles, *Phys. Rev. Lett.* **110**, 084101 (2013).
 - [13] M. Puschmann, P. Cain, M. Schreiber, and T. Vojta, Multifractal analysis of electronic states on random Voronoi-Delaunay lattices, *Eur. Phys. J. B* **88**, 314 (2015).
 - [14] S. Bhattacharjee, P. Sierant, M. Dudziński, J. Wehr, J. Zakrzewski, and M. Lewenstein, Anderson localization induced by structural disorder, *Phys. Rev. B* **111**, L180202 (2025).
 - [15] M. Titov and H. Schomerus, Nonuniversality of Anderson localization in short-range correlated disorder, *Phys. Rev. Lett.* **95**, 126602 (2005).
 - [16] P. Lugan and L. Sanchez-Palencia, Localization of Bogoliubov quasiparticles in interacting Bose gases with correlated disorder, *Phys. Rev. A* **84**, 013612 (2011).
 - [17] I. V. Gornyi, A. D. Mirlin, and D. G. Polyakov, Interacting electrons in disordered wires: Anderson localization and low- T transport, *Phys. Rev. Lett.* **95**, 206603 (2005).
 - [18] D. Basko, I. Aleiner, and B. Altshuler, Metal-insulator transition in a weakly interacting many-electron system with localized single-particle states, *Ann. Phys.* **321**, 1126 (2006).
 - [19] I. L. Aleiner, B. L. Altshuler, and G. V. Shlyapnikov, A finite-temperature phase transition for disordered weakly

- interacting bosons in one dimension, *Nat. Phys.* **6**, 900 (2010).
- [20] V. P. Michal, I. L. Aleiner, B. L. Altshuler, and G. V. Shlyapnikov, Finite-temperature fluid–insulator transition of strongly interacting 1D disordered bosons, *Proc. Natl. Acad. Sci. USA* **113**, E4455 (2016).
- [21] F. Alet and N. Laflorencie, Many-body localization: An introduction and selected topics, *C. R. Phys.* **19**, 498 (2018).
- [22] J. Billy, V. Josse, Z. Zuo, A. Bernard, B. Hambrecht, P. Lugan, D. Clément, L. Sanchez-Palencia, P. Bouyer, and A. Aspect, Direct observation of Anderson localization of matter waves in a controlled disorder, *Nature (London)* **453**, 891 (2008).
- [23] G. Roati, C. D’Errico, L. Fallani, M. Fattori, C. Fort, M. Zaccanti, G. Modugno, M. Modugno, and M. Inguscio, Anderson localization of a non-interacting Bose–Einstein condensate, *Nature (London)* **453**, 895 (2008).
- [24] M. Schreiber, S. S. Hodgman, P. Bordia, H. P. Lüschen, M. H. Fischer, R. Vosk, E. Altman, U. Schneider, and I. Bloch, Observation of many-body localization of interacting fermions in a quasirandom optical lattice, *Science* **349**, 842 (2015).
- [25] P. G. Harper, Single band motion of conduction electrons in a uniform magnetic field, *Proc. Phys. Soc. Sect. A* **68**, 874 (1955).
- [26] M. Y. Azbel, Quantum particle in one-dimensional potentials with incommensurate periods, *Phys. Rev. Lett.* **43**, 1954 (1979).
- [27] S. Aubry and G. André, Analyticity breaking and Anderson localization in incommensurate lattices, *Ann. Israel Phys. Soc.* **3**, 18 (1980).
- [28] G. Domínguez-Castro and R. Paredes, The Aubry–André model as a hobbyhorse for understanding the localization phenomenon, *Eur. J. Phys.* **40**, 045403 (2019).
- [29] S. Iyer, V. Oganesyan, G. Refael, and D. A. Huse, Many-body localization in a quasiperiodic system, *Phys. Rev. B* **87**, 134202 (2013).
- [30] V. Mastropietro, Localization of interacting fermions in the Aubry–André model, *Phys. Rev. Lett.* **115**, 180401 (2015).
- [31] D. D. Vu and S. Das Sarma, Moiré versus Mott: Incommensuration and interaction in one-dimensional bichromatic lattices, *Phys. Rev. Lett.* **126**, 036803 (2021).
- [32] H. Yao, T. Giamarchi, and L. Sanchez-Palencia, Lieb–liniger bosons in a shallow quasiperiodic potential: Bose glass phase and fractal Mott lobes, *Phys. Rev. Lett.* **125**, 060401 (2020).
- [33] Y. Wang, C. Cheng, X.-J. Liu, and D. Yu, Many-body critical phase: Extended and nonthermal, *Phys. Rev. Lett.* **126**, 080602 (2021).
- [34] M. Gonçalves, B. Amorim, F. Riche, E. V. Castro, and P. Ribeiro, Incommensurability enabled quasi-fractal order in 1D narrow-band moiré systems, *Nat. Phys.* **20**, 1933 (2024).
- [35] P. Mognini, Stability of quasicrystalline ultracold fermions to dipolar interactions, *Phys. Rev. Res.* **7**, L032026 (2025).
- [36] P. Mognini and B. Chakrabarti, Stability of dipolar bosons in a quasiperiodic potential, *Phys. Rev. Res.* **7**, 023237 (2025).
- [37] H. Yao, L. Tanzi, L. Sanchez-Palencia, T. Giamarchi, G. Modugno, and C. D’Errico, Mott transition for a Lieb–Liniger gas in a shallow quasiperiodic potential: Delocalization induced by disorder, *Phys. Rev. Lett.* **133**, 123401 (2024).
- [38] K. O. Rasmussen, T. Cretegny, P. G. Kevrekidis, and N. Grønbech-Jensen, Statistical mechanics of a discrete nonlinear system, *Phys. Rev. Lett.* **84**, 3740 (2000).
- [39] C. Orzel, A. Tuchman, M. Fenselau, M. Yasuda, and M. Kasevich, Squeezed states in a Bose–Einstein condensate, *Science* **291**, 2386 (2001).
- [40] M. Greiner, O. Mandel, T. Esslinger, T. W. Hänsch, and I. Bloch, Quantum phase transition from a superfluid to a Mott insulator in a gas of ultracold atoms, *Nature (London)* **415**, 39 (2002).
- [41] A. Polkovnikov, S. Sachdev, and S. M. Girvin, Nonequilibrium Gross–Pitaevskii dynamics of boson lattice models, *Phys. Rev. A* **66**, 053607 (2002).
- [42] T. Mithun, Y. Kati, C. Danieli, and S. Flach, Weakly nonergodic dynamics in the Gross–Pitaevskii lattice, *Phys. Rev. Lett.* **120**, 184101 (2018).
- [43] S. Lellouch and L. Sanchez-Palencia, Localization transition in weakly interacting Bose superfluids in one-dimensional quasiperiodic lattices, *Phys. Rev. A* **90**, 061602(R) (2014).
- [44] Y. Wang, J.-H. Zhang, Y. Li, J. Wu, W. Liu, F. Mei, Y. Hu, L. Xiao, J. Ma, C. Chin *et al.*, Observation of interaction-induced mobility edge in an atomic Aubry–André wire, *Phys. Rev. Lett.* **129**, 103401 (2022).
- [45] J. D. Bodyfelt, D. Leykam, C. Danieli, X. Yu, and S. Flach, Flatbands under correlated perturbations, *Phys. Rev. Lett.* **113**, 236403 (2014).
- [46] S. Ganeshan, J. H. Pixley, and S. Das Sarma, Nearest neighbor tight binding models with an exact mobility edge in one dimension, *Phys. Rev. Lett.* **114**, 146601 (2015).
- [47] C. Danieli, J. D. Bodyfelt, and S. Flach, Flat-band engineering of mobility edges, *Phys. Rev. B* **91**, 235134 (2015).
- [48] L. Sanchez-Palencia, Smoothing effect and delocalization of interacting Bose–Einstein condensates in random potentials, *Phys. Rev. A* **74**, 053625 (2006).
- [49] P. Lugan, D. Clément, P. Bouyer, A. Aspect, and L. Sanchez-Palencia, Anderson localization of Bogolyubov quasiparticles in interacting Bose–Einstein condensates, *Phys. Rev. Lett.* **99**, 180402 (2007).
- [50] A. Padhan, M. K. Giri, S. Mondal, and T. Mishra, Emergence of multiple localization transitions in a one-dimensional quasiperiodic lattice, *Phys. Rev. B* **105**, L220201 (2022).
- [51] M. Gonçalves, B. Amorim, E. V. Castro, and P. Ribeiro, Renormalization group theory of one-dimensional quasiperiodic lattice models with commensurate approximants, *Phys. Rev. B* **108**, L100201 (2023).
- [52] N. Bogoliubov, On the theory of superfluidity, *J. Phys. (USSR)* **11**, 23 (1947).
- [53] L. Morales-Molina, E. Doerner, C. Danieli, and S. Flach, Resonant extended states in driven quasiperiodic lattices: Aubry–André localization by design, *Phys. Rev. A* **90**, 043630 (2014).
- [54] D. R. Hofstadter, Energy levels and wave functions of Bloch electrons in rational and irrational magnetic fields, *Phys. Rev. B* **14**, 2239 (1976).
- [55] K. Ino and M. Kohmoto, Critical properties of Harper’s equation on a triangular lattice, *Phys. Rev. B* **73**, 205111 (2006).
- [56] L. Gong and P. Tong, Fidelity, fidelity susceptibility, and von neumann entropy to characterize the phase diagram of an extended Harper model, *Phys. Rev. B* **78**, 115114 (2008).
- [57] A. Avila, S. Jitomirskaya, and C. A. Marx, Spectral theory of extended Harper’s model and a question by Erdős and Szekeres, *Invent. Math.* **210**, 283 (2017).